Soliman *et al.*
Journal of Engineering and Applied Science (2024) 71:46
https://doi.org/10.1186/s44147-024-00381-2

Journal of Engineering and Applied Science

RESEARCH Open Access

Arching mechanism for large span flexible culverts with shallow soil covers

Nashwa Nabil Soliman[1*], Sherif Adel Yahia Akl[2], Ahmed Hosny Abdel Rahman[1] and Sherif Ahmed Mourad[3]

*Correspondence: Nashwa.Soliman.J@eng-st.cu.edu.eg

[1] Department of Civil Engineering, National Research Centre, Giza, Egypt
[2] Soil Mechanics & Foundation Research Laboratory, Faculty of Engineering, Cairo University, Giza, Egypt
[3] Department of Structural Engineering, Faculty of Engineering, Cairo University, Giza, Egypt

Abstract

Soil-steel composite bridges (SSCBs) use the surrounding soil and the culvert's flexible corrugated steel thin plates to support vertical loads above the culvert. Existing codes use empirical equations based on field measurements and full-scale tests for small and ordinary span SSCBs to estimate the arching process and how it distributes vertical stresses on the culvert walls. The empirical equations then compute the design straining actions. Recent developments in construction technology and urbanization have led to a significant increase in typical spans of SSCBs. This paper investigates large span SSCBs and the associated induced arching action using three-dimensional finite element analysis (FEA). The study compares the FEA findings of straining actions for large span SSCB case studies to the calculations of valid design codes. The comparison demonstrates that existing codes fail to predict the real arching mechanism and, consequently, the resulting straining actions. In addition, the FEA results illustrate how the arching mechanism varies as the span changes. Arching action is typically positive for relatively small spans but becomes negative as the span increases. Finally, results prove that current codes cannot accurately predict real arching, leading to inappropriate design straining actions. For large span SSCBs, these codes require modifications for the arching factors and the profile aspect ratio factors.

Keywords: Soil-steel composite bridges (SSCB), Large span culverts, Corrugated steel plates, Arching mechanism, Induced straining actions, Profile aspect ratio, Finite element model

Introduction

The corrugated metal flexible culverts' first usage was for sewage and drainage design. They were deeply buried and had small diameters. With time, their development and utilization were to serve as pedestrian and vehicular underpasses with shallower covers and larger diameters. The ease and speed of installation, the inherent strength of corrugated steel, sustainability, and esthetics all contribute to the widespread usage of this style of culverts. They present a viable alternative to bridge infrastructure, which is a considerable contributor to greenhouse gas emissions because of the massive raw material and energy consumption during their whole life cycle [1].

Soil-steel composite bridge (SSCB) main characteristic is a unique method of providing the load bearing capacity as opposed to ordinary culverts. The surrounding soil for

ordinary concrete, stone, and brick culverts is regarded only as a way of transmitting loads. However, for SSCBs, the surrounding soil plays a significant role in sustaining the loads with the culvert, known as soil structure interaction. Therefore, the arching mechanism takes place. The arching is the pressure or load transfer between the backfill soil layers above the culvert that arises from the culvert walls' flexibility. As a result, the design of buried culverts entails identifying the best culvert cross-section and the surrounding soil properties [2].

Arching plays a prime role in SSCB performance. Arching may be positive or negative. Positive arching occurs when the backfilling soil around the culvert has the potential to disperse the load away from the culvert. That is because the majority of the load disperses across soil layers. Consequently, the induced normal forces in the culvert cross-section are less than in the case of no arching. Negative arching occurs when the culvert is stiffer than the backfilling soil, so more load transfers to the culvert. Hence, the induced normal forces increase. Thus, the arching mechanism must be well-estimated during the design of SSCBs.

Various countries have released design manuals/codes for SSCB design and construction specifications. These codes give empirical equations based on field and laboratory experiments for small and regular span SSCBs. In general, the design codes concentrate on two main design concepts. These are the geotechnical features of steel culvert construction, such as excavation, filling, cover depth, and installation, as well as the structural aspects, such as profile, corrugation depth, deformations, straining actions, and bolted connections.

Ring compression is the prime design requirement in some design codes. Ring compression force is the main straining action for designing a culvert with a small span and high soil cover. However, when the span increases, the soil cover decreases, or using deep corrugated cross-sections, deformations and bending moments develop due to the cause of backfilling construction loads and traffic loads acting over the shallowly buried soil steel structure. Therefore, it is crucial to carefully evaluate the bending moments and displacements for large span SSCBs. Most available design manuals can assist in estimating the straining actions acting on the SSCB under specific situations. These manuals govern the minimum cover depth, backfill properties, corrugated steel plate properties, and culvert profile aspect ratio. However, to keep up with the rapid rise in the usage of large span SSCB, these design manuals need to be updated [3–5].

Many previous numerical studies investigated SSCBs in several topics, while they were for SSCBs with spans up to 18 m. Recently constructed SSCBs have spans larger than 18 m. The Ostróda SSCB in Poland has a 25.5 m span [3]. As well as the Shammal Bridge in UAE has a 32.66 m span [6]. Therefore, this paper investigates large span SSCBs with spans up to 32.66 m with deep corrugated steel plates and explores the effect of a large span on the induced arching mechanism. It presents a study on six large span field case studies using three-dimensional finite element model analysis. FEA output soil movement contours investigate the effect of span increase on the induced arching mechanism. In addition, FEA results of induced straining actions due to backfilling loads are compared to the corresponding calculated values using two different design codes. The study highlights the factors for each code responsible for estimating the SSCB arching mechanism and influencing the accuracy of the calculated values. The study aims to

check these codes' validity for estimating the real arching and reasonable design straining actions for large span SSCBs.

Overview of the Canadian and Swedish design concepts for SSCBs

Nowadays, two of the most popular and used design codes for designing SSCBs are the Canadian highway bridge design code CHBDC [7] and the Swedish soil-steel composite bridges SDM [8]. Each code defines parameters and factors with some design limitations to calculate straining actions induced in corrugated steel plate cross-section. Herein, the paper highlights the approaches each code adopts and how these approaches could affect the prediction of large span SSCB performance.

First, the CHBDC [7] design provisions are based on the Ontario Highway Bridge Design Code (OHBDC) with some updates to be applicable across Canada [9]. CHBDC includes section #7 (buried structures), which presents the design of SSCB structures with spans ≥ 3 m, where the design is based on ultimate state principles. The design equations were derived firstly for shallow corrugated plates 152×51 mm (pitch by depth), and then they were adapted for application to all corrugation sizes [9]. The code defines a minimum cover height requirement to guarantee that the culvert design is influenced only by normal forces while neglecting bending moments [10]. The minimum permitted cover height is based on the culvert profile, effective span (D_h), and effective rise (D_v). However, the code allows shallower cover heights, not less than 0.6 m, with deep corrugated plates as long as considering bending moments in the design.

Maximum normal force (T_D) equation (Eq. 1) considers the factor (A_f) and the relative axial stiffness (C_s) into account for computing the maximum normal force acting on the culvert wall from the initial stage of construction. The A_f value depends on the effective span (D_h), effective rise (D_v), and cover height, where the code estimates the value of A_f for a range of $0.6 \leq D_h/D_v \leq 1.6$. Then, the arching factor is defined as $(1-0.1C_s)\ A_f$ and multiplied by half the applied soil load (0.5^*W).

$$T_D = 0.5(1 - 0.1C_s)A_f W \tag{1}$$

Meanwhile, the bending moment (M_D) equation (Eq. 2) has two portions, one calculating the moment generated by side backfilling (M_1) and the other calculating the moment generated by top backfilling (M_B). In general, side backfilling causes a higher bending moment, as adding additional side backfilling layers increases the bending moment. Then, adding the top backfilling layers reverses the induced bending moment direction and decreases the overall bending moment. Therefore, the design should consider the higher bending moment. The bending moment due to side backfilling (M_1) equation (Eq. 3) includes factors K_{M1} and R_B. K_{M1} is a function of the relative bending stiffness (N_F), while R_B is a function of the profile aspect ratio ($D_v/2D_h$).

$$M_D = M_1 + M_B \tag{2}$$

$$M_1 = K_{M1} R_B \gamma {D_h}^3 \tag{3}$$

Next, SDM [8] is also known as the Pettersson-Sundquist design method. SDM calculations are based on fundamental theories that were compared and calibrated with

full-scale field tests [11]. SDM includes a set of limitations and assumptions concerning culvert profile geometry, backfilling soil type, and relative stiffness (λ_f) between the backfilling soil and the steel culvert ($100 \leq \lambda_f \leq 50{,}000$). Additionally, it specifies a minimum cover height of 0.5 m for road bridge culverts and 1 m for railway bridge culverts. Minimal cover aims to reduce the possibility of local failure under concentrated loads. The SDM design process considers normal forces and bending moments generated on corrugated steel plates for all corrugation types.

The SDM normal force equation (Eq. 4) has two portions: one for the normal force generated by side backfilling and one for the normal force generated by top backfilling. The SDM, unlike CHBDC, does not include the impact of the relative axial stiffness component in its equation. Also, it considers the arching effect (S_{ar}) only for the part calculating normal force due to top backfilling.

$$N_{soil,k} = 0.2\frac{H}{D}\rho_{surr}D^2 + S_{ar}(0.9\frac{h}{D} - 0.5\frac{h}{D}\frac{H}{D})\rho_{cover}D^2 \tag{4}$$

However, the SDM bending moment equation has two portions in the same manner as CHBDC. The bending moment due to side backfilling ($M_{soil,k}$) equation (Eq. 5) considers the factors $f_{2,surr}$, f_1, and f_3. $f_{2,surr}$ is a function of the relative bending stiffness (λ_f), while f_1 and f_3 are functions in the profile aspect ratio (H/D).

$$M_{soil,k} = D^3\rho_{surr}f_1f_3f_{2,surr} \tag{5}$$

In general, neither the CHBDC nor the SDM design approaches spell out the maximum span for SSCB. However, both codes specify limitations on the proposed equations' parameters based on small and regular span SSCBs [5]. Table 1 summarizes a comparison between both codes regarding the limitations and the parameters used in calculating straining actions.

Methods

Finite element analysis (FEA) description

The author uses the multipurpose finite element program PLAXIS 3D [12] to study the behavior of large span SSCB. The FEA results are used to evaluate the effect of

Table 1 CHBDC and SDM comparison

	CHBDC	SDM
Span limitations	Not exist	
Profile limitations	$R_t/R_s \leq 5$	$R_t/R_s \leq 4$
Minimum cover height	0.6 m	0.5 m (road bridges) 1 m (railway bridges)
Soil steel relative stiffness limitation	Not exist	$100 < \lambda_f < 50{,}000$
Maximum normal force equation	Function of: • Profile aspect ratio • Soil cover height • Backfill soil density and Young's modulus • Steel section axial stiffness	Function of: • Profile aspect ratio • Soil cover height • Backfill soil density and friction angle
Maximum bending moment equation	Function of: • Profile aspect ratio • Backfill soil density and Young's modulus • Steel section bending stiffness	

span on the induced arching mechanism. Then, they are compared to CHBDC and SDM calculations to check the capability of these codes to estimate reasonable design straining actions.

The study includes six SSCBs with spans between 9.5 and 32.66 m. The culverts are double radii open arched profiles with deep corrugated steel plates. Figure 1 shows their schematics with detailed dimensions. They have shallow cover heights, where the h/D equals 0.09 for all cases. In addition, Table 2 summarizes each culvert profile and cross-section data. The backfill soil for all SSCBs is assumed to be medium sand verged with silty sand layered each 0.3 m. The backfill properties are according to the values reported by Korusiewicz [13]. It has 50 MPa Young's modulus, 18.54 kN/m^3 dry density, and 35° friction angle.

Figure 2 illustrates the finite element (FE) model used to simulate the investigated open-arched SSCBs consisting of the culvert and the surrounding soil medium. The choice of the material models for the backfilling soil and the corrugated steel plates is based on previous research that specifies the appropriate models defined in FE simulation for the backfilling soil and corrugated steel plates. PLAXIS 3D library allows

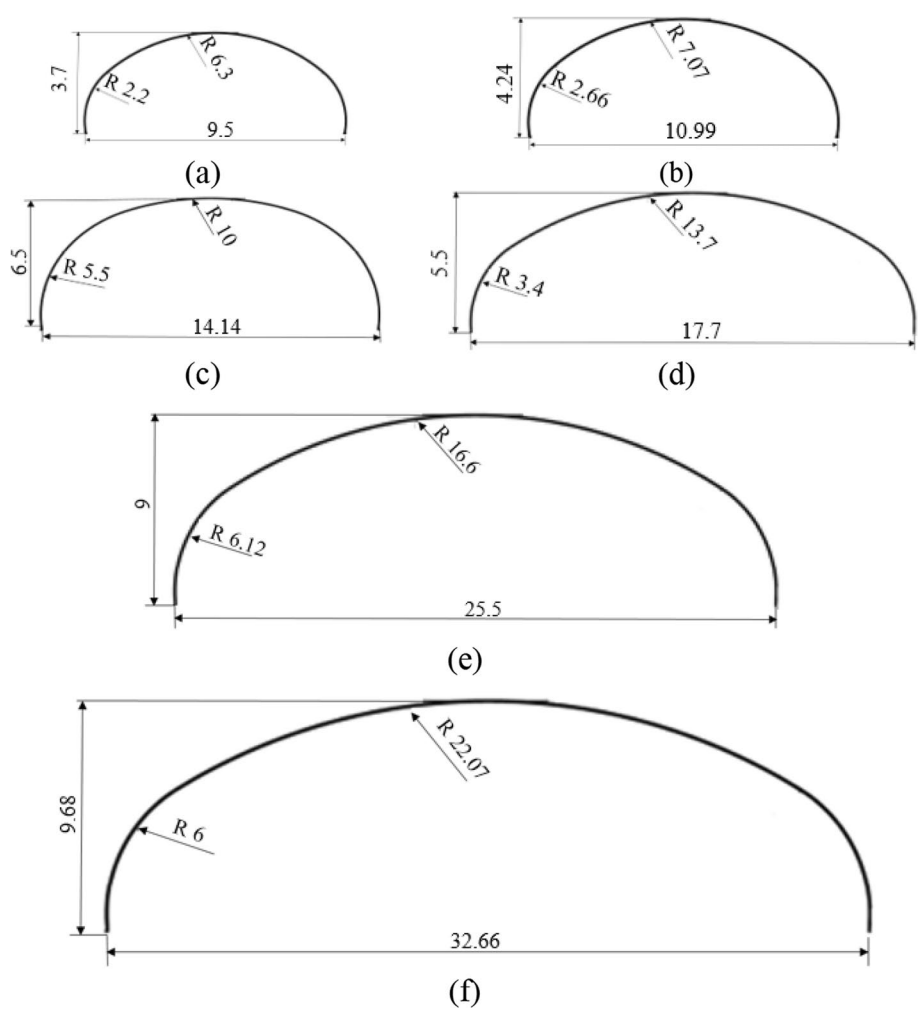

Fig. 1 Schematic of the modeled field case studies (all dimensions are in meters)

Table 2 Geometry of the SSCBs case studies

Span *D* (m)	9.5	10.99	14.14	17.7	25.5	32.66
Rise *H* (m)	3.7	4.24	6.5	5.5	9	9.68
Cover height *h* (m)	0.9	1	1.3	1.6	2.2	2.81
Corrugation (mm)			381x140		500x237	
Plate thickness (mm)			7		9.65	12

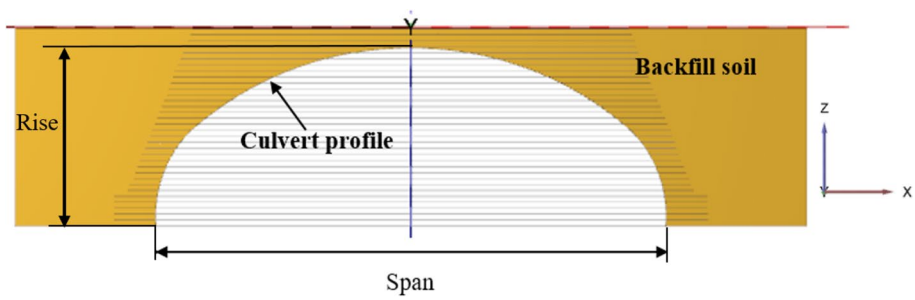

Fig. 2 Soil-steel composite bridge FEA model

soil simulation using the hardening soil (HS) material model that can simulate the soil stress-dependent stiffness considering the effect of compaction-induced loads from the soil to the culvert [14, 15]. On the other hand, the use of orthotropic plates for simulating corrugated steel plates was approved by previous research to provide reliable results [14, 16]. Using orthotropic elastoplastic plates allows for the reduction of the required number of elements in the FE model. They are a subset of anisotropic materials,their properties vary depending on the measurement direction. As a result, they have three planes/axes of symmetry and a poisons ratio of zero ($\nu_{equ.}$). Their properties are calculated according to the method developed by Orod and Siavash [17]. Tables 3 and 4 summarize the values used in FEA for the HS backfilling soil model and the orthotropic steel plates, respectively.

The boundary conditions are fixed in both directions at the model base and horizontally fixed at the edges. The mesh size is medium for the whole SSCB FE model, and the mesh coarseness is refined for the culvert plates and the soil next to the culvert walls. The reason is to account for the close spacing between the backfilling soil model and the culvert model steel plates and to save time during analysis by minimizing the number of FE model elements.

Construction stages and compaction loads simulation

SSCB construction in situ is staged construction. The staged construction starts with installing the corrugated steel plate to form the culvert profile. That is followed by placing the compacted backfilling soil layers on both sides of the culvert equally to ensure contact between the plates and the soil.

PLAXIS 3D finite element program can simulate the construction stages through a series of phases. The model's initial phase presents the state before construction (i.e., no geometry is active). Then, the model's first phase presents the installation of the

Table 3 Backfilling soil HS model parameters used in FEA

Material model		Hardening soil
Material type		**Drained**
General properties	γ_{unsat} (kN/m^3)	18.54
	γ_{sat} (kN/m^3)	18.54
Stiffness	E_{ref} (kN/m^2)	50,000
	E_{oed} (kN/m^2)	48,000
	E_{ur} (kN/m^2)	150,000
	m	0.5
Strength	c_{ref} (kN/m^2)	0.02
	$\Phi°$	35°
	$\psi°$	5°
Interfaces strength (R_{inter})		0.8

Table 4 Orthotropic steel plates parameters used in FEA

Corrugated plate dimensions (mm)		381x140x7	500x237x9.65	500x237x12
Equivalent thickness (m)		0.1676	0.2766	0.2770
Equivalent unit weight (kN/m^3)		4.273	3.985	4.950
Equivalent Young's modulus (longitudinal) (E_1) (kN/m^2)		15,300	8915	17,030
Equivalent Young's modulus (circumferential) (E_2) (kN/m^2)		11,360,000	10,592,260	13,160,000
Shear modulus in plane (G12) (kN/m^2)		160,400	118,188	182,000
Shear moduli out of plane (kN/m^2)	**G13**	5886	3429	6551
	G23	4,369,000	4,073,950	5,060,000

corrugated steel plates forming the culvert profile by activating the corrugated steel plates and their interfaces. Next, the following model phases present the soil backfilling stages by activating each backfilling layer with its accompanying compaction load through sequential phases till reaching the road level. The compaction load is simulated as vertical surface loading equal to 20 kN/m^2 for side backfilling [18], then its value is reduced for the top layers of backfill until the ground level. Figure 3 presents a sample FEA model simulation of the backfilling stages with corresponding compaction loads.

Regarding the reported case studies, there is no information about groundwater onsite. Therefore, the water table is assumed to be below the foundation level.

FE model verification

The Wildlife overpass SSCB field measurements are compared to the FEA results to verify the FE model. The Wildlife overpass has a 17.7 m span, a 5.5 m rise, and a 2 m cover height [13]. Figure 4 proves that the FEA results are reasonable compared to field measurements. However, the normal force values of FEA results are higher than field measurements. The reason can be that some measuring sensors suffered high temperatures in the field, which resulted in false readings, especially for measurements due to side backfilling. Korusiewicz mentioned that the measured normal forces changed erratically at different points [13]. Maximum field measurements for normal force and bending moment were recorded as − 610 kN/m and 52 kNm/m, respectively. Meanwhile, the FEA results for both straining actions are − 690 kN/m and 53 kNm/m.

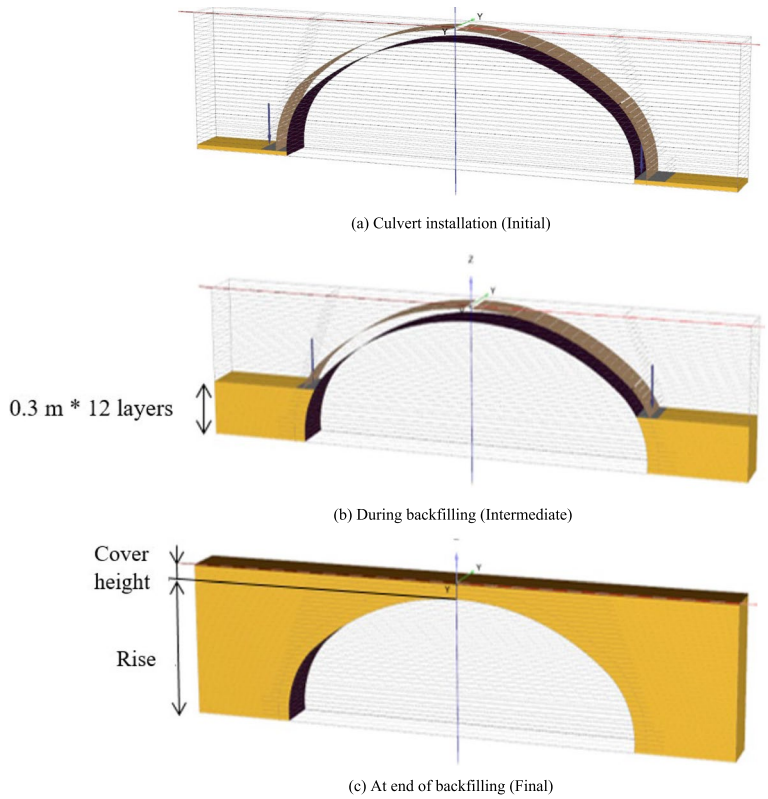

Fig. 3 FEA staged construction

Results and discussion

PLAXIS 3D models are calculated, and the results are used to investigate the effect of span increase on arching mechanism, deformations, and induced straining actions. Then, the FEA results are compared with the corresponding calculated values using available design codes.

Arching mechanism

The arching mechanism has a master role in transferring the loads to the culvert cross-section. As mentioned, an arching mechanism may be positive or negative depending on the relative stiffness between the backfilling soil and the culvert's corrugated steel cross-section.

The arching mechanism can be presented numerically by the movement contours of the soil concerning the culvert. Therefore, Fig. 5 plots the soil movement contours generated by PLAXIS 3D output to illustrate the type of induced arching mechanism at the end of backfilling for the case studies. The figure clarifies that an increase in span greatly influences the arching mechanism type. It shows that for spans up to 10.99 m, the contours prove the occurrence of positive arching. Then, for larger spans, the arching is inverted to be negative. In addition, the soil wedge supported on the culvert walls expands as the span increases, which is the main reason that the straining actions increase significantly with the span increase.

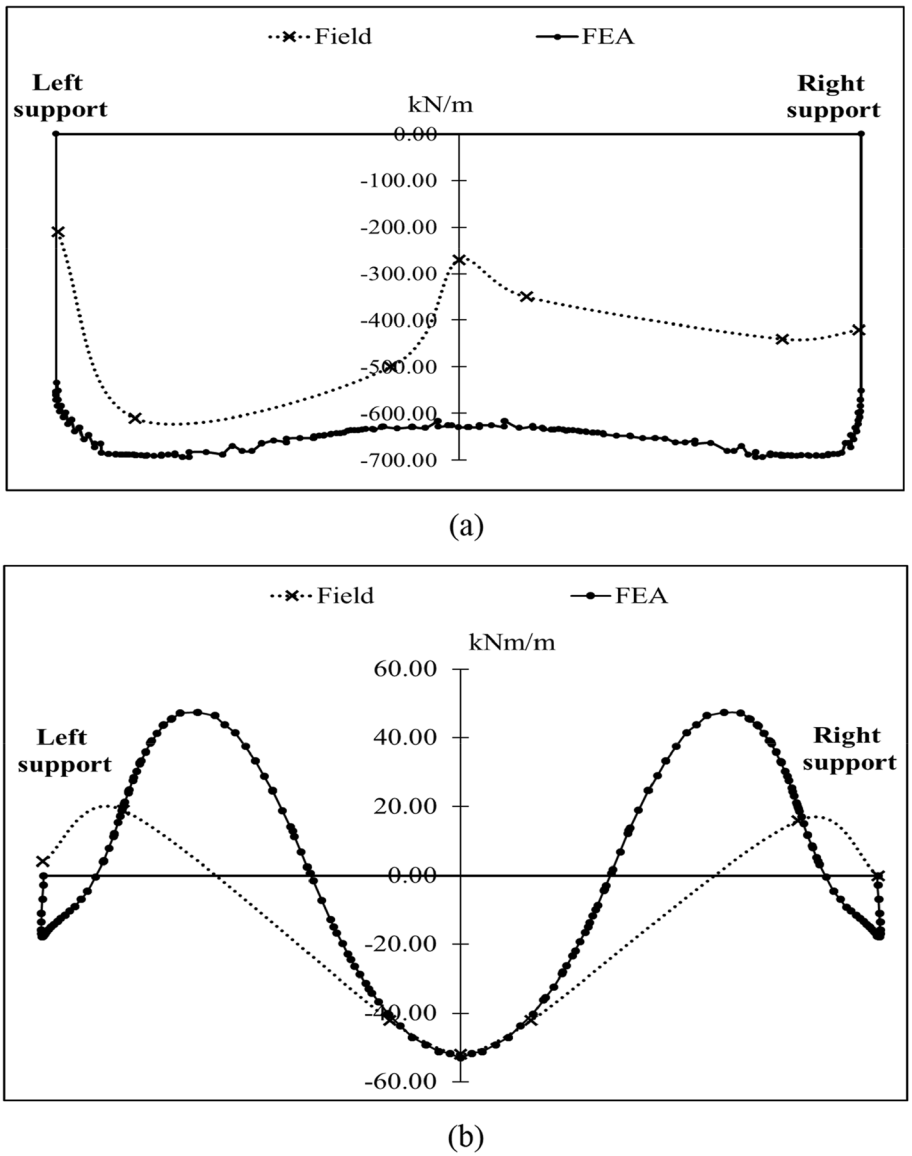

Fig. 4 Wildlife overpass field measurements and FEA results: **a** maximum normal forces (kN/m) and **b** maximum bending moments (kNm/m)

Accordingly, the studied culverts are classified into two groups as follows: positive arching SSCBs (i.e., culverts with spans equal to 9.5 and 10.99 m) and negative arching SSCBs (i.e., culverts with spans equal to 14.14, 17.7, 25.5, and 32.66 m).

Deformations

Results show that the span increase and corresponding induced arching mechanism influence the maximum vertical deformations (U_{zmax}). The positive arching SSCBs maximum vertical deformations are 6.4 mm and 14 mm for spans 9.5 m and 10.99 m, respectively. The negative arching SSCBs maximum vertical deformations are 49 mm, 78 mm, 125 mm, and 275 for spans 14.14, 17.7, 25.5, and 32.66, respectively. Results prove that as the arching mechanism changes from positive to negative when the span changes from 10.99 to 14.14 m, the maximum culvert vertical deformation increases

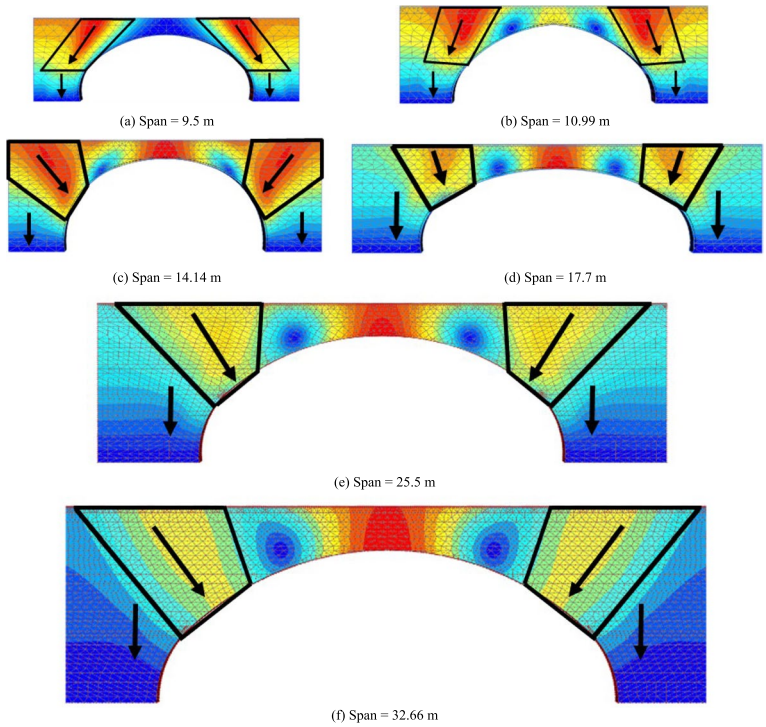

Fig. 5 Surrounding soil movement at the end of backfilling for the six case studies

by 3.5 times (i.e., $(U_{zmax})_{14.14}/(U_{zmax})_{10.99} = 49/14 = 3.5$). In addition, maximum deformation results illustrate that the deformation value for span 32.66 m increased by 43 times more than that for span 9.5 m.

Regarding the design codes, the CHBDC states that any upward or downward deformations should not exceed 2% of the culvert rise. On the other hand, the SDM does not mention a vertical deformation limit. Thus, the maximum vertical deformation to rise ratio is computed for each culvert and compared with the CHBDC limit.

Figure 6 demonstrates each culvert maximum vertical deformation to rise ratio (U_{zmax}/H). The deformation ratios change from 0.17 to 2.84% with the increase in span. The figure shows that the maximum vertical deformation to rise ratio for span 32.66 m exceeds the CHBDC limit. Therefore, large span SSCBs with negative arching should be carefully monitored during construction to avoid excessive and undesirable deformations.

Straining actions

The culvert cross-section is subjected to different straining actions. The two main straining actions are the normal force and the bending moment induced about the cross-section strong axis (circumferential direction). The normal force maximum value occurs at the end of backfilling. On the other hand, the maximum bending moment value occurs when the backfilling layers reach the crown point. Figures 7 and 8 plot the FEA results due to dead loads only (backfill soil load) for normal force and bending moment distribution along the culvert's span, respectively, for both the positive and negative arching SSCBs. The figures represent the culvert length by unity for all case studies to plot different span culvert results. Both figures confirm that span and corresponding induced

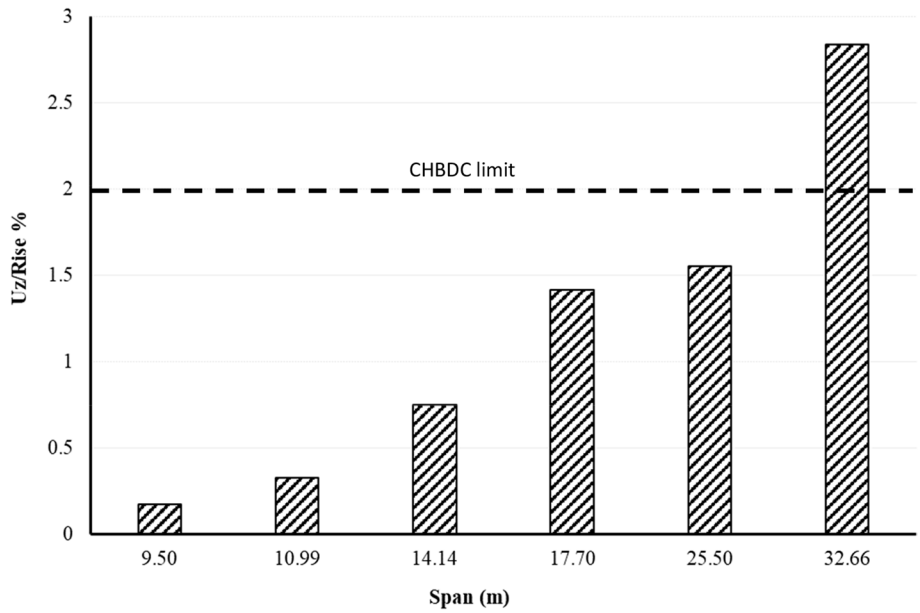

Fig. 6 Maximum Vertical deformation to rise ratio with different spans

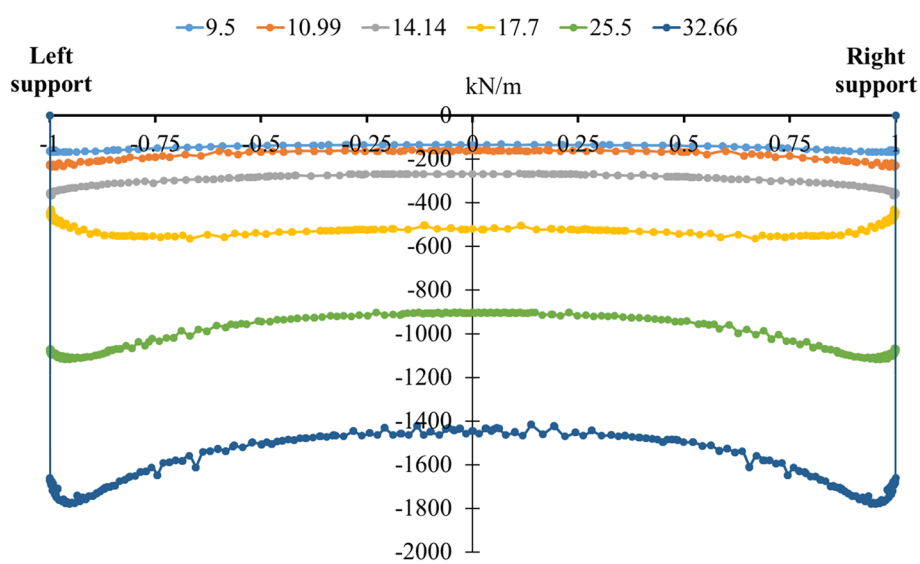

Fig. 7 FEA Normal force distribution along each culvert span at the end of backfilling (kN/m)

arching mechanism type greatly influence the induced straining actions, as they are directly proportional to the span increase. Besides, Fig. 7 shows that the normal forces for positive arching SSCBs slightly vary (i.e., spans 9.5 and 10.99 m). However, for negative arching SSCBs, there is a significant change in the values of the normal force by span increase. That is because of the soil wedge increase supported on the culvert wall.

Regarding the location of maximum straining action, Fig. 7 clarifies that the maximum normal force location does not vary as the span increases. It occurs within a quarter of the span on both sides near the supports. Similarly, Fig. 8 illustrates that for the different

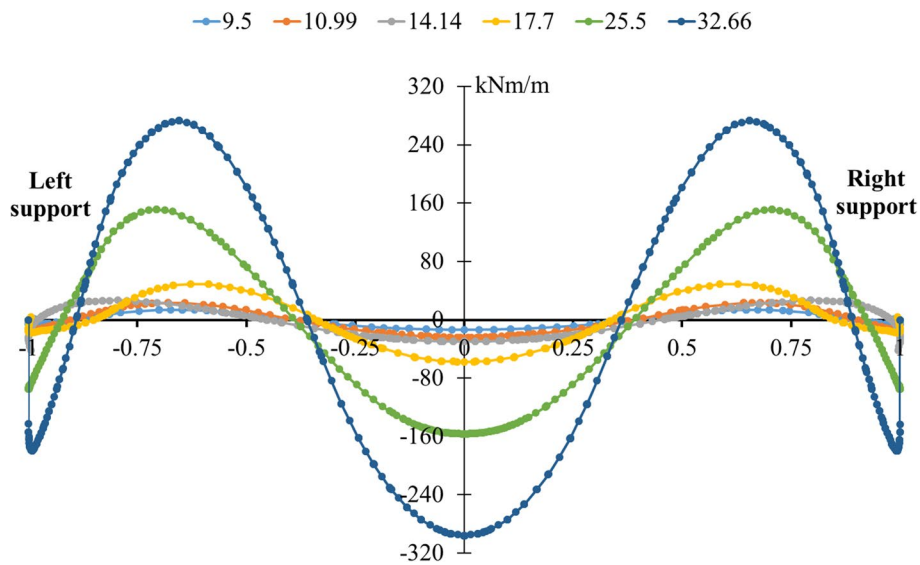

Fig. 8 FEA Bending moments distribution along each culvert span at the end of backfilling (kNm/m)

spans, maximum bending moments frequently occur at the crown and shoulders, with about the same values but in opposing directions.

FEA results vs design codes calculated values

Existing codes propose equations based on small and ordinary span SSCBs. Hence, the CHBDC and SDM are used to calculate the straining actions acting on the corrugated steel plates for both the positive and negative arching SSCBs studied cases. Then, calculated values are compared with the corresponding FEA results. Figures 9 and 10 plot the normal forces and bending moments, respectively, calculated by both codes and the maximum results from FEA. A general conclusion from both curves is that calculated values are not mostly compatible (overestimated or underestimated) with FEA results for large span culverts.

Since the span increase has a direct influence on the arching mechanism type. Therefore, overestimated/underestimated calculated straining actions are a reason for the failure of codes to estimate the true arching mechanism that takes place between backfilling soil and the large span culvert. As a result, they estimate that the culvert supports either more or less of the original applied loads. In addition, some codes' equations do not account for the impact of relative stiffness between the backfilling soil and the corrugated steel plates, which consequently affects the results. Therefore, each code equations are thoroughly investigated to identify their imperfections regarding large span SSCB design.

Normal forces codes equations

Regarding normal forces, Fig. 9 illustrates that normal forces calculated by CHBDC are always less than those calculated by SDM. In addition, CHBDC provides mostly well-estimated normal forces compared to FEA results. The CHBDC calculations range

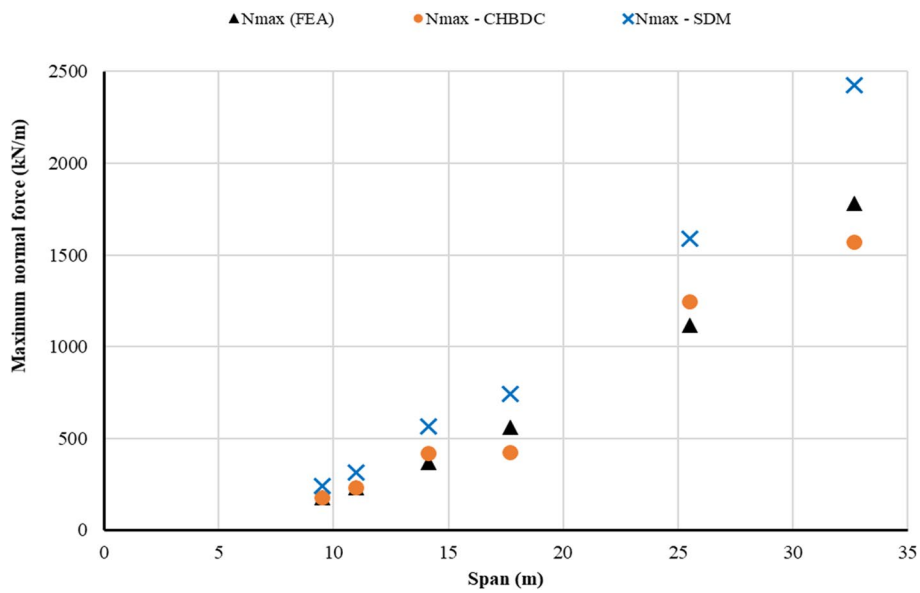

Fig. 9 Code calculations and FEA results for maximum normal force (kN/m)

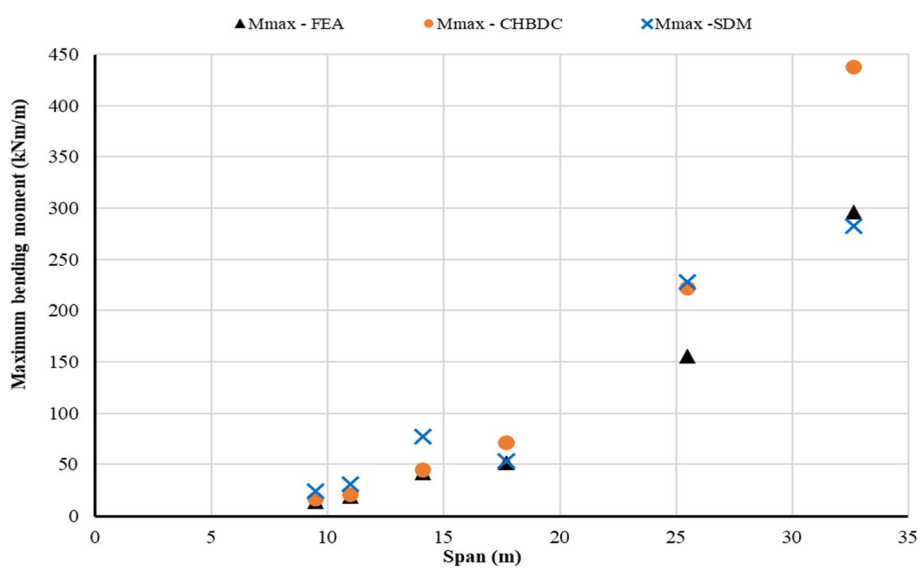

Fig. 10 Code calculations and FEA results for maximum bending moment (kNm/m)

between 0.75 and 1.14 times the FEA results. On the contrary, SDM calculated values are always more than FEA results, ranging between 1.32 and 1.54 times the FEA results.

Even that Fig. 9 shows that CHBDC normal force equation sometimes can estimate close values to FEA results, the figure also illustrates that the same equation cannot estimate appropriate values for some cases. Calculated normal forces for positive arching SSCBs are compatible with FEA results, while for negative arching SSCBs, calculated values vary from FEA results. Therefore, the discussion will highlight the arching factor defined by the code's equation. CHBDC presents the arching factor by the following

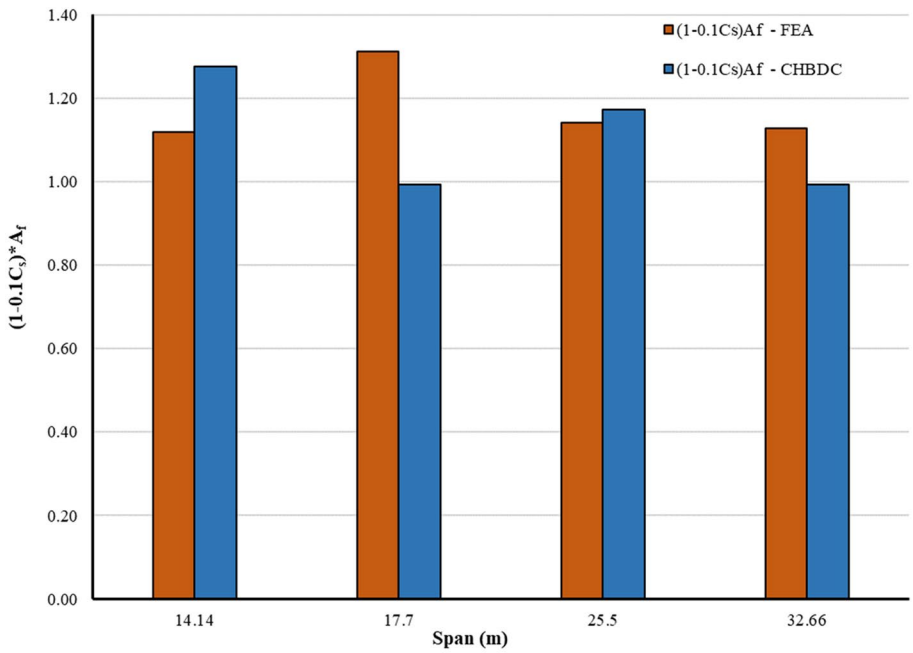

Fig. 11 FEA and CHBDC arching factors ($(1-0.1C_s)\ A_f$) for the negative arching SSCBs

Eq. $(1-0.1C_s)\ A_f$. This code assumes that the arching effect starts from the beginning of the backfilling stages, as it is multiplied by the whole soil load surrounding the culvert.

Figure 11 plots the arching factor calculated by CHBDC and recalculated from FEA results for the negative arching SSCBs. The figure shows that the code estimated arching factor is less accurate, especially when using a small corrugated steel cross-section (i.e., 381*140*7 mm). For example, for the culvert with a span of 17.7 m and corrugated plates 381*140*7 mm, the arching factor calculated by the code is 25% less than that recalculated from FEA results. Also, for the culvert with a span of 32.66 m and corrugated plates 500*237*12, the arching factor calculated by the code is 14% less than the recalculated value from FEA results. This notable difference between the arching factor calculated by CHBDC and recalculated from FEA results for both mentioned spans can be due to A_f curves, as they are limited to $0.6 \leq D_h/D_v \leq 1.6$ only, where the D_h/D_v for spans 17.7 and 32.66 are 1.6 and 1.687, respectively. Therefore, the CHBDC should modify the arching factor equation/parameters for large span culverts.

Next, the SDM design code presents the arching factor S_{ar}, which is a function of the cover soil friction angle, cover height, and culvert span. SDM normal force equation has two portions, one to calculate the normal force due to side backfilling and the other for that due to top backfilling. The S_{ar} factor is considered only for the portion calculating normal force due to top backfilling. Figure 12 plots the calculated and resulting normal forces divided according to that induced due to side backfilling only and top backfilling only. That is to find in which portion the problem of overestimating the calculated normal force occurs. The figure clarifies that the SDM overestimates the normal force due to side backfilling load where the values reach up to 90% more than FEA results that increases the total estimated normal force due to dead load. On the other hand, the calculated values due to top backfilling are well-estimated compared to FEA results.

Therefore, the SDM should modify the normal force equation due to side backfilling for large span culverts by considering the arching factor effect and the relative axial stiffness effect between soil and steel plates.

Bending moments codes equations

Regarding bending moments, as the maximum value occurs when backfilling reaches the crown level, therefore the equation portion evaluated in both codes is only concerned with calculating moments induced by side backfilling. The study considers the absolute bending moment because steel has the same bending stiffness in both directions, so the moment direction does not influence it.

Figure 10 illustrates that both codes' calculated values vary between well-estimated and overestimated values. CHBDC overestimated values reach up to 48% more than FEA results, while SDM overestimated values reach up to 83% more than FEA results.

Regarding the CHBDC, the bending moment equation depends on two main factors K_{M1} and R_B. K_{M1} is a function of the relative bending stiffness between the soil and the steel plates (N_F), while R_B is a function of profile aspect ratio ($D_v/2D_h$). Table 5 summarizes the $D_v/2D_h$ for each culvert, the corresponding calculated R_B, and the ratio between the code calculated values and FEA results. The table shows that for culverts with profile aspect ratios $0.2 \leq D_v/2D_h \leq 0.35$, the calculated bending moments are significantly higher than FEA results, where the difference is 48% for the culvert with a span of 32.66 m. For culverts with aspect ratios $0.35 < D_v/2D_h \leq 0.5$, the calculated bending moment values are more than FEA results with an acceptable difference of less than 10%. Figure 13 plots the R_B calculated by the code and the recalculated from FEA results. The figure illustrates that the R_B equation for $0.2 \leq D_v/2D_h \leq 0.35$ should be modified to reduce

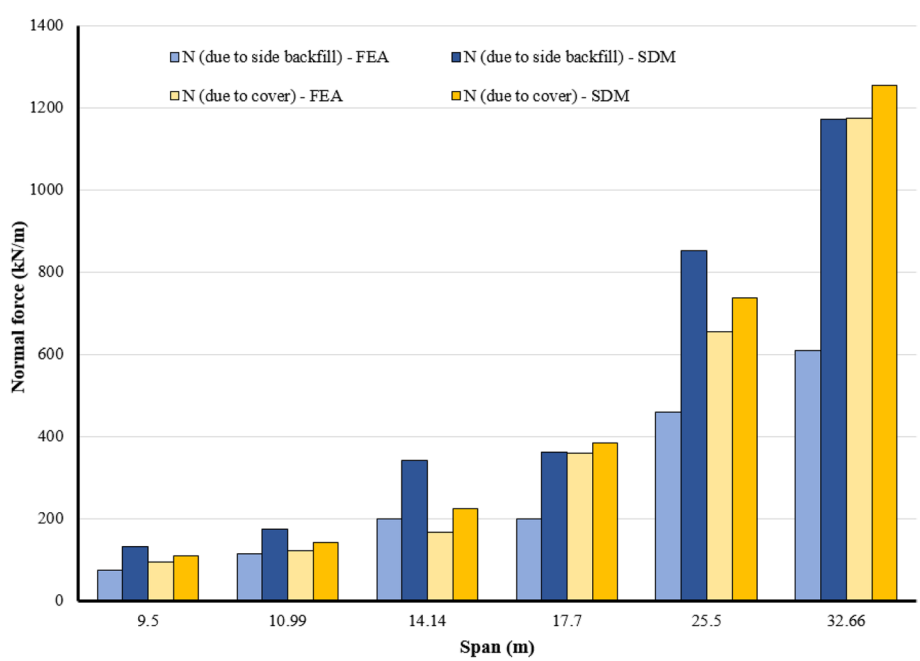

Fig. 12 Normal forces divided due to side and top backfilling FEA results and SDM calculations

Table 5 CHBDC R_B factor and the ratio between maximum calculated bending moment to FEA result

Span *D* (m)		**9.5**	**10.99**	**14.14**	**17.7**	**25.5**	**32.66**
$D_v/2D_h$		0.39	0.39	0.46	0.31	0.35	0.3
$R_B=$	$0.67+0.87[(D_v/2D_h)-0.2]$ for $0.2 \le D_v/2D_h \le 0.35$	0.85	0.85	0.95	0.77	0.80	0.75
	$0.8+1.33[(D_v/2D_h)-0.35]$ for $0.35 < D_v/2D_h \le 0.5$						
	D_v/D_h for $D_v/2D_h > 0.5$						
$(\text{CHBDC/FEM})_{\text{max. bending moment}}$		1.10	1.08	1.07	1.37	1.42	1.48

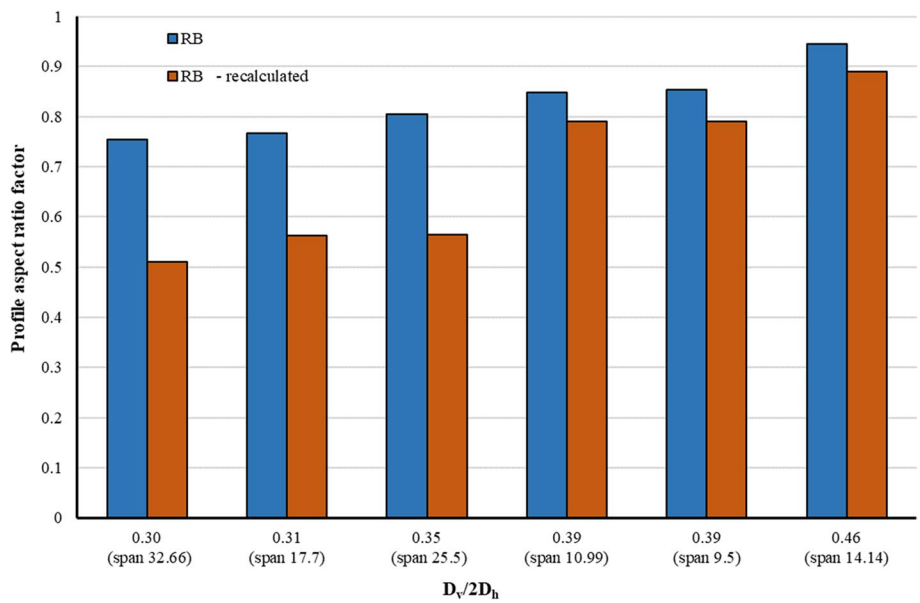

Fig. 13 Profile aspect ratio calculated by the CHBDC (R_B) and recalculated from FEA results ($R_{B\text{-}recalculated}$)

the calculated R_B value. For the case study with a 32.66 m span and 0.3 profile aspect ratio, the R_B value shall be reduced by 33%.

On the other hand, the SDM equation calculates bending moment due to side backfilling depending on three main factors $f_{2,surr}$, f_1, and f_3, where $f_{2,surr}$ is a function of the relative stiffness (λ_f) between the soil and the steel plates. The other two factors are function of the profile aspect ratio (H/D). Generally, the SDM equation is similar to that CHBDC equation but multiplied by an additional factor f_3. Table 6 summarizes the H/D for each culvert, the corresponding calculated factors (f_1 and f_3), and the ratio between code calculated values and FEA results. The code equation has a problem in estimating the arching mechanism for large span culverts with profile aspect ratios (H/D) greater than or equal to 0.35. The overestimated calculated values reached up to 83% of the FEA results. The product of aspect ratio factors (f_1*f_3) is recalculated from FEA results for each SSCB. Then, they are plotted versus the code calculated values, as shown in Fig. 14. The figure clarifies that for the case study with a span of 14.14 m and $H/D=0.46$, the factors shall be reduced by 27%. Therefore, f_1 and f_3 equations require modifications for large span SSCBs with corresponding rise to span ratios equal to or greater than 0.35.

Table 6 SDM f_1 and f_3 factors and the ratio between maximum calculated bending moment to FEA result

Span *D* (m)		**9.5**	**10.99**	**14.14**	**17.7**	**25.5**	**32.66**
H/D		0.39	0.39	0.46	0.31	0.35	0.3
$f_1 =$	$0.67 + 0.87[(H/D) - 0.2]$ for $0.2 \le H/D \le 0.35$ $0.8 + 1.33[(H/D) - 0.35]$ for $0.35 < H/D \le 0.5$ $2\ H/D$ for $H/D > 0.5$	0.85	0.85	0.95	0.77	0.80	0.75
$f_3 = 6.67(H/D) - 1.33$		1.27	1.27	1.74	0.74	1	0.67
$(SDM/FEM)_{max.\ bending\ moment}$		1.60	1.59	1.83	1.02	1.46	0.96

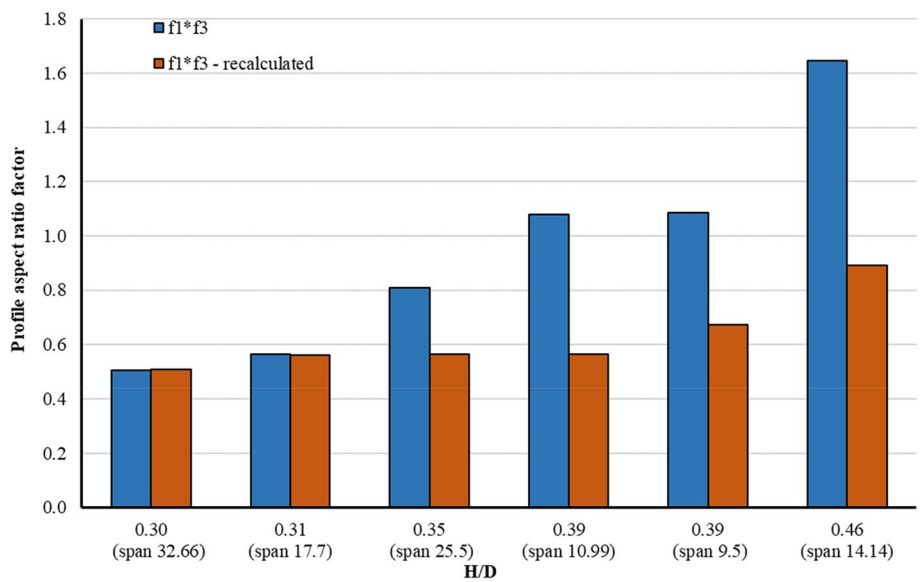

Fig. 14 Profile aspect ratio calculated by the SDM (f_1*f_3) and recalculated from FEA results (f_1*$f_{3\text{-}recalculated}$)

As a result of the prior discussion, codes' equations that calculate arching factors and profile aspect ratio factors should be modified for large span culverts. The codes should consider the arching impact from the beginning of backfilling and the relative stiffness between backfilling soil and corrugated steel plates (i.e., axial stiffness and bending stiffness). Hence, the culvert and the backfilling soil interact during the construction stages.

Conclusions

Recent developments in construction technology and urbanization have led to a significant increase in typical spans of SSCBs. Therefore, this paper illustrates a numerical analysis study that explores the effect of large spans on the arching mechanisms around the SSCB. Finite element analysis demonstrates the limitations of the existing calculation methods in CHBDC and SDM.

The study investigates six SSCB field case studies using PLAXIS 3D. The SSCBs have open arched culverts with spans 9.5 m up to 32.66 m. Firstly, FEA results for the Wildlife overpass [13] are verified using field measurements. Then, the study evaluates the FEA results for the associated soil movement representing the arching mechanism and the induced vertical deformations. Next, normal forces and bending

moments FEA results are displayed. Lastly, using CHBDC and SDM, normal forces and bending moments are calculated and compared to FEA results. The investigation yields the following conclusions:

- The arching mechanism is significantly affected by span and profile aspect ratio. For case studies with spans of 9.5 and 10.99 m, the FEA soil movement contours prove that positive arching occurs. On the other hand, the FEA soil movement contours show that negative arching takes place for larger spans. Moreover, the contours show that the area of the supported soil wedge is significantly affected by the profile aspect ratio and the span.
- As the span increases and negative arching occurs, the maximum vertical deformation relative to the culvert rise ratio increases significantly. In the case of negative arching SSCB with a span of 32.66 m, for example, the (U_{zmax}/rise) ratio is 2.84%, which exceeds the CHBDC limit (2%). As a result, it is crucial to monitor large span culverts for deformations during construction to avoid any undesired deformations.
- Induced straining actions are significantly affected by span since their values increase as span increases.
- FEA results prove that normal forces for positive arching SSCBs slightly vary with the change in span. On the contrary, for negative arching SSCBs, there is a significant change in the values of the normal forces by span increase. That is because of the soil wedge increase supported on the culvert wall.
- The calculated normal forces by CHBDC for large span culverts fluctuate between well-estimated for positive arching SSCBs and far estimated in case of negative arching SSCBs. The explanation is that the CHBDC arching factor equation cannot present the real arching mechanism. In addition, the A_f factor curves are limited to $0.6 \leq D_h/D_v \leq 1.6$ only, while for spans 17.7 and 32.66 m the $D_h/D_v \geq 1.6$. On the other hand, SDM always overestimates the calculated normal forces. The reason is that the SDM equation neglects the effect of relative axial stiffness between the backfilling soil and the corrugated steel plates. Also, it ignores the arching influence in the equation portion calculating normal force due to side backfilling. Consequently, the calculated normal forces due to side backfilling exceed the FEA results by ratios up to 90%, reflected in the total calculated normal force value.
- Both codes cannot accurately estimate the maximum induced bending moment due to side backfilling of some investigated case studies. The reason is common for both codes, which is the improper proposed equations for calculating the profile aspect ratio factors for large span culverts. This results in overestimated calculated bending moments up to 48% for CHBDC and 83% for the SDM.
- For large span SSCBs, the CHBDC and SDM equations should be modified to capture their actual performance and offer well-estimated straining actions for their design.

Abbreviations

D_h [m]	Effective culvert span @ CHBDC
D_v [m]	Effective culvert rise @ CHBDC
T_D [kN/m]	Maximum thrust in a conduit wall per unit length due to dead loads @ CHBDC
A_f	Factor for calculating dead normal force @ CHBDC

C_s	Relative axial stiffness @ CHBDC
W [kN/m]	Dead weight of the soil column above a culvert per unit length @ CHBDC
M_D [kNm/m]	Moment in the wall of a soil-metal structure due to a dead load @ CHBDC
M_1 [kNm/m]	Moment in a soil-metal structure resulting from fill to the crown level @ CHBDC
M_B [kNm/m]	Additional moment in the wall of a soil-metal structure due to a height of fill above the crown @ CHBDC
k_{M1}	Factor used in calculating moments due to side backfilling only in soil-metal structures @ CHBDC
N_F	Relative bending stiffness @ CHBDC
R_B	Profile aspect ratio effect @ CHBDC
λ_f	Relative stiffness between the backfilling soil and the steel culvert @ SDM
γ [kN/m^3]	Unit weight of soil @ CHBDC
$N_{soil,k}$ [kN/m]	Normal force due to soil load @ SDM
ρ_{surr} [kN/m^3]	Weight density of the soil material up to the height of the crown @ SDM
ρ_{cover} [kN/m^3]	Weight density of the soil material above the height of the crown @ SDM
S_{ar}	Arching factor @ SDM
$M_{soil,k}$ [kNm/m]	Moment due to soil load @ SDM
f_1 and f_3	Profile aspect ratio factors @ SDM
D [m]	Culvert span @ SDM
H [m]	Culvert rise @ SDM
h [m]	Backfilling soil cover height for open arched profiles supported on concrete footings @ SDM
R_s [m]	Arched profile side radius
R_t [m]	Arched profile top radius

Acknowledgements
Not applicable.

Authors' contributions
NS performed the software analysis, interpreted the results, and wrote/edited the paper manuscript. SA revised the modeling technique, criticized the results, determined the paper organization, and revised the technical writing of the manuscript. AH and SM revised and approved the research approach, design of the work plan, and the final version of the manuscript. All authors read and approved the final manuscript.

Funding
The authors did not receive support from any organization for the submitted work.

Availability of data and materials
The datasets used and/or analyzed during the current study are available from the corresponding author on request.

Declarations

Competing interests
The last author, Prof. Sherif Ahmed Mourad, is an associate editor for the *Journal of Engineering and Applied Science*.

Received: 12 December 2023 Accepted: 3 February 2024
Published online: 20 February 2024

References

1. Du G, Pettersson L, Karoumi R (2018) Soil-steel composite bridge: an alternative design solution for short spans considering LCA. J Clean Prod 189:647–661 https://www.sciencedirect.com/science/article/abs/pii/S0959652618311132
2. Madaj A (2017) Buried flexible steel structures. Key problems of design code study. Arch Inst Civ Eng 23:11–20
3. Machelski C, Tomala P, Kunecki B, Korusiewicz L, Williams K, El-Sharnouby M (2017) Ultracor – 1st realization in Europe, design, erection, testing. Archives of Institute of Civil Engineering 23: 189–197. https://doi.org/10.21008/j.1897-4007.2017.23.18
4. Mahgoub A, El Naggar H (2018) Effect of the cross-sectional rigidity on the static and seismic behaviour of CSP culverts. Proceedings of the 3rd world congress on civil, structural and environmental engineering (CSEE'18), Budapest, Hungary. https://doi.org/10.11159/icgre18.153
5. Wadi A, Pettersson L (2017) Large-span soil-steel composite bridges. Arch Inst Civ Eng 23:287–292. https://doi.org/10.21008/j.1897-4007.2017.23.26
6. AIL project profile (2019) http://www.ail.ca/wp-content/uploads/2019/03/AIL-000-project-profiles_v5_Digitalnov2019update.pdf
7. CHBDC (2014) Canadian highway bridge design code. CAN/CSA-S6–06, Canadian Standards Association International, Mississauga, Ontario
8. Pettersson L, Sundquist H (2015) Design of steel composite bridges. TRITA-BKN report 112 5th edition, ISSN 1103 – 4289, KTH Royal Institute of Technology, Stockholm
9. Finlay S, Biro P, Ahmed H (2003) Soil-steel structures and the Canadian highway bridge design code. Annual conference of the Transportation Association of Canada. https://www.tac-atc.ca/en/conference/papers/soilsteel-structures-and-canadian-highway-bridge-design-code

10. CSPI (2007) Corrugated steel pipe institute. Handbook of steel drainage and highway construction products. 2nd Canadian edition 2007
11. Wadi A (2012) Soil steel composite bridges. Master of Science Thesis, Stockholm
12. PLAXIS 3D Reference Manual (2020) Connect edition V20.03 https://communities.bentley.com/cfs-file/__key/communityserver-wikis-components-files/00-00-00-05-58/PLAXIS3DCE_2D00_V20.03_2D00_2_2D00_Reference.pdf
13. Korusiewicz L (2015) Testing of a large-span soil-shell structure without stiffeners during backfilling process. Roads and Bridges 14:175–190
14. El Naggar H, Campbell A, Ezzeldin I (2021) Effect of the employed material model on the predicted behaviour of corrugated metal pipes. Transportation Research Record Journal of the Transportation Research Board 2675 (10). https://doi.org/10.1177/03611981211016461
15. Mahgoub A, El Naggar H (2020) Coupled TDA–geocell stress-bridging system for buried corrugated metal pipes. Journal of Geotechnical and Geoenvironmental Engineering 146 (7), American Society of Civil Engineers, ISSN 1090–0241. https://doi.org/10.1061/(ASCE)GT.1943-5606.0002279
16. Elshimi T (2011) Three dimensional nonlinear analysis of deep corrugated steel culverts. Doctoral Thesis in the Department of Civil Engineering, Queen's University
17. Aagah O, Aryannejad S (2014) Dynamic analysis of soil-steel composite railway bridges. MSc Thesis in the Department of Civil and Architectural Engineering, Royal Institute of Technology. https://www.diva-portal.org/smash/get/diva2:761372/FULLTEXT01.pdf
18. Ezzeldin I, El Naggar H (2022) Numerical modelling of induced stresses in buried corrugated metal structures due to compaction efforts. Transp Geotech 32. https://doi.org/10.1016/j.trgeo.2021.100706

Publisher's Note